Nonlinear drift resonance between charged particles and ultra-low frequency waves: Theory and Observations

Li Li[1], Xu-Zhi Zhou[1], Yoshiharu Omura[2], Zi-Han Wang[1,3], Qiu-Gang Zong[1], Ying Liu[1], Yi-Xin Hao[1], Sui-Yan Fu[1], Margaret G. Kivelson[4], Robert Rankin[5], Seth G. Claudepierre[6], and John R. Wygant[7]

Corresponding author: X.-Z. Zhou, School of Earth and Space Sciences, Peking University, Beijing, China. (xuzhi.zhou@gmail.com)

[1]School of Earth and Space Sciences,

In Earth's inner magnetosphere, electromagnetic waves in the ultra-low frequency (ULF) range play an important role in accelerating and diffusing charged particles via drift resonance. In conventional drift-resonance theory,

Peking University, Beijing, China.

[2]Research Institute for Sustainable Humanosphere, Kyoto University, Kyoto, Japan.

[3]Department of Climate and Space Sciences and Engineering, University of Michigan, Ann Arbor, Michigan, USA.

[4]Department of Earth, Planetary, and Space Sciences, University of California, Los Angeles, California, USA.

[5]Department of Physics, University of Alberta, Edmonton, Alberta, Canada.

[6]Space Science Applications Laboratory, The Aerospace Corporation, El Segundo, California, USA.

[7]School of Physics and Astronomy, University of Minnesota, Minneapolis, Minnesota, USA.

linearization is applied under the assumption of weak wave-particle energy exchange so particle trajectories are unperturbed. For ULF waves with larger amplitudes and/or durations, however, the conventional theory becomes inaccurate since particle trajectories are strongly perturbed. Here, we extend the drift-resonance theory into a nonlinear regime, to formulate nonlinear trapping of particles in a wave-carried potential well, and predict the corresponding observable signatures such as rolled-up structures in particle energy spectrum. After considering how this manifests in particle data with finite energy resolution, we compare the predicted signatures with Van Allen Probes observations. Their good agreement provides the first observational evidence for the occurrence of nonlinear drift resonance, highlighting the importance of nonlinear effects in magnetospheric particle dynamics under ULF waves.

1. Introduction

In Earth's magnetosphere, ultra-low frequency (ULF) pulsations in Pc 4-5 frequency range (2-22 mHz) often exhibit properties of standing shear Alfven waves [*Cummings et al.*, 1969; *Chen and Hasegawa*, 1974; *Southwood*, 1974; *Takahashi and McPherron*, 1984; *Kivelson and Southwood*, 1985; *Anderson et al.*, 1990]. These transverse waves can effectively accelerate or decelerate charged particles as a result of wave-particle drift resonance [*Southwood and Kivelson*, 1981, 1982]. When such a resonance occurs, the azimuthal drift speed of a resonant particle matches the wave propagation speed, and the particle experiences a constant phase of the wave electric field. This process enables a sustained energy exchange between ULF waves and charged particles, which provides a major source of particle acceleration and diffusion in the Van Allen radiation belts [*Mann et al.*, 2013; *Liu et al.*, 2016; *Sarris et al.*, 2017; *Zong et al.*, 2017].

According to the theory developed by *Southwood and Kivelson* [1981, 1982], the characteristic signatures of drift resonance is the 180°-phase difference between particle flux oscillations across the resonant energy. Such signatures have been identified by in-situ observations [*Zong et al.*, 2007, 2009; *Claudepierre et al.*, 2013; *Dai et al.*, 2013; *Foster et al.*, 2015], providing clear evidence on the presence of drift-resonant interactions in the inner magnetosphere. The conventional theory has been further extended to take into account temporal [*Zhou et al.*, 2015, 2016] and spatial distributions [*Li et al.*, 2017b; *Hao et al.*, 2017] of ULF waves, which predicts increasingly tilted stripes in the energy spectrum. Recent spacecraft observations have also shown evidence in support of these predicted signatures [*Zhou et al.*, 2016; *Li et al.*, 2017a; *Li et al.*, 2017b].

In the aforementioned studies, a linearization approach is utilized by assuming that particle trajectories are unperturbed despite their energy gain or loss from ULF waves. This assumption is appropriate only if the particle energy variation is much smaller than its initial energy. For ULF waves with large amplitudes and/or long durations, the large wave-particle energy exchange can modify the particle trajectory to cause significant nonlinear effects [*Wang et al.*, 2018]. The nonlinear particle behavior within ULF waves have been discussed in *Elkington et al.* [2003], to analyze the role of ULF waves in accelerating and diffusing particles in an asymmetric, compressed magnetosphere. Nonlinear particle trajectories have been also studied in magnetohydromagnetic models of ULF waves [*Degeling et al.*, 2007, 2008], which highlight the effect of ULF waves with finite spatial and temporal extents over the profile of electron phase space density (PSD). According to *Degeling et al.* [2008], nonlinear drift resonance may produce localized peaks in electron PSD, a phenomenon previously attributed almost exclusively to electron interactions with very low frequency (VLF) waves [*Summers et al.*, 1998; *Horne et al.*, 2005; *Chen et al.*, 2007; *Li et al.*, 2014].

These studies have provided new insights into how nonlinear drift resonance may change the particle dynamics in a coupled magnetospheric system, although there lacks a direct observational evidence for the occurrence of such nonlinear interactions in the magnetosphere. In this paper, we aim to develop the nonlinear drift resonance theory based on these previous studies, to formulate nonlinear particle trapping in a wave-carried potential well, and accordingly to predict the observable signatures of nonlinear wave-particle in-

teractions. The predicted signatures are then compared with data from Van Allen Probes to provide the first observational identification of nonlinear drift resonance.

2. Theory of nonlinear drift resonance

Let us consider an equatorially mirroring, nonrelativistic particle in Earth's magnetic dipole field. For simplicity, we follow *Southwood and Kivelson* [1981] to assume that the ULF waves of interest are poloidal-mode waves (with magnetic and electric field oscillations in radial and azimuthal directions, respectively) propagating azimuthally. In other words, the wave electric field in the equatorial plane can be expressed by

$$\boldsymbol{E} = E_\phi \sin(m\phi - \omega t)\hat{\boldsymbol{e_\phi}}, \tag{1}$$

where E_ϕ represents the wave amplitude, ϕ is magnetic longitude (increasing eastward), m is the azimuthal wave number (either positive or negative, depending on eastward or westward directions of wave propagation), and ω is the wave angular frequency. The wave also carries a magnetic field oscillation (to satisfy Faraday's law). However, its amplitude near the equator is usually weak for the wave with significant equatorial electric field (fundamental-mode or odd-harmonic ULF waves), and therefore the effect of the magnetic field oscillation on the particle behavior is neglected in this study. Since the particle drifts in the azimuthal direction, the gyro-averaged rate of its energy gain from the ULF wave equals

$$\frac{dW}{dt} = \omega_d L R_E \cdot q E_\phi \sin(m\phi - \omega t), \tag{2}$$

where W is the particle kinetic energy, L is the L-shell parameter, R_E is Earth's radius, and ω_d is the particle's azimuthal drift frequency. According to *Northrop* [1963], ω_d can

be expressed by

$$\omega_d = \frac{d\phi}{dt} = -\frac{3LW}{qB_E R_E^2}, \tag{3}$$

where B_E is the equatorial magnetic field on Earth's surface. Note that the sign of ω_d depends on q, which corresponds to the eastward/westward drift motion of negatively/positively-charged particles.

The W-dependence of (3) suggests that the particle trajectory differs significantly from the unperturbed orbit when the particle's energy variation becomes comparable to its initial energy [*Wang et al.*, 2018]. Therefore, the linearization approach in *Southwood and Kivelson* [1981] can no longer be applied in these cases. Moreover, the particle's L-location also depends on W given the constance of the first adiabatic invariant μ in ULF wave field (since the ULF wave period is much larger than particle gyroperiod). In other words, particles being accelerated/decelerated would move radially inward/outward. In Earth's magnetic dipole, the L-location of the particle can be given by

$$L = \left(\frac{\mu B_E}{W(t)}\right)^{1/3}. \tag{4}$$

Substituting (4) into (3), we obtain

$$\omega_d = \frac{d\phi}{dt} = -\frac{3\mu^{1/3} W^{2/3}(t)}{qB_E^{2/3} R_E^2}. \tag{5}$$

Utilizing (2) and (4), we next obtain the time derivative of (5) as

$$\frac{d\omega_d}{dt} = -\frac{2\mu^{1/3} W^{-1/3}}{qB_E^{2/3} R_E^2} \cdot \frac{dW}{dt} = \frac{6\mu E_\phi}{qB_E R_E^3} \sin(m\phi - \omega t). \tag{6}$$

We point out here that equation (6) does not depend on ω_d, which eliminates the nonlinearity in (2) and enables an analytical solution for the particle motion in ULF wave field.

The system can be further simplified by introducing two variables,

$$\zeta = m\phi - \omega t, \tag{7}$$

$$\theta = \frac{d\zeta}{dt} = m\omega_d - \omega, \tag{8}$$

which represent the phase of the particle location in the wave rest frame and its time derivative, respectively. Note that when θ equals zero, the particle drifts at the same speed as the waves and satisfies the drift resonant condition. Based on (6), (7) and (8), we have

$$\frac{d^2\zeta}{dt^2} = \frac{d\theta}{dt} = \frac{6m\mu E_\phi}{qB_E R_E^3} \cdot \sin\zeta, \tag{9}$$

which has the same format as the pendulum equation of motion as long as m/q is negative (valid when we study positively/negatively-charged particle behavior in westward/eastward-propagating waves). The pendulum equation suggests that near-resonant particles (with small enough $|\theta|$ values) could be trapped in a wave-carried potential well centred at $\zeta = 0°$. The trapping frequency of particles in the potential well, based on a small-angle approximation ($\sin\zeta \ll 1$), is given by

$$\omega_{tr} = (-\frac{6m\mu E_\phi}{qB_E R_E^3})^{1/2}, \tag{10}$$

which is proportional to the square root of the wave amplitude. For particles beyond the small-angle approximation, the trapping frequency can still be expressed in terms of elliptic integrals, which becomes much lower for marginally-trapped particles. Similar pictures of particle trapping in potential wells carried by other plasma waves (such as Langmuir waves) have been discussed in many plasma physics textbooks (interested readers may refer to *Gurnett and Bhattacharjee* [2005, Chapter 8] for details).

One may also formulate the particle trajectories in the ζ-θ phase space. To do this, we eliminate t from (8) and (9), to have

$$\theta d\theta = -\omega_{tr}^2 \sin\zeta d\zeta, \tag{11}$$

and its integral gives

$$\theta^2 = 2\omega_{tr}^2 \cos\zeta + C, \tag{12}$$

in which C is determined by the initial θ and ζ values of any given particle. To better understand this equation, we present in Figures 1a and 1e examples of electron phase-space trajectories when these electrons interact with ULF waves of different amplitudes (1 and 6 mV/m, respectively). Here the horizontal and vertical axes represent the ζ and θ values of the sample electrons. These electrons, with the initial phase-space location indicated by colored circles, are launched at the same ζ location of $-90°$ with the same μ but different θ values. Given a fixed μ, the θ values have one-to-one correspondence to particle energy (see (5)) and to the L-location (see (4)). Therefore, we can also show in Figures 1b and 1f the electron energy as functions of ζ, and in Figures 1c and 1g the corresponding L variations. Also shown in Figures 1d and 1h are the profiles of the wave electric field (the blue lines) and their azimuthal integral (the effective electrostatic potential, the red lines). The shaded and non-shaded areas represent the regions where electrons are decelerated (moving downward in θ and in energy, upward in L in the phase-space diagram) and accelerated, respectively.

Let us focus on the difference between the trapped and untrapped trajectories. Electrons with θ always higher than 0 (the magenta and the purple lines in Figure 1a, and the purple line in Figure 1e) keep moving to the right since they always drift faster than the waves

($m\omega_d > \omega_r$). Electrons with lower energies (the orange and the green lines in Figure 1a, and the green line in Figure 1e) keep moving to the left as they have $m\omega_d < \omega_r$. The sample electrons launched at the resonant energy (the blue circles), on the other hand, are accelerated at first since they are initially located in the non-shaded area, and the acceleration corresponds to an enhancement of their drift speeds (now greater than the wave speed). Therefore, in Figures 1a and 1e, these electrons move upward in θ and rightward in ζ until they reach the shaded area at 0° and start to be decelerated (moving to the lower right). After that, at 90°, the energies of the electrons drop back to the resonant energy, and they start to move to the lower left. Eventually, these electrons return to their initial locations to form closed trajectories in phase space. As we have pointed out, such closed orbits can be equivalently understood as electrons trapped within a wave-carried potential well ($-180° < \zeta < 180°$). Moreover, if we increase the wave electric field (as in Figure 1h), the potential well becomes deeper (compare Figures 1d and 1h) so electrons with initial energies much higher or lower than the resonant energy (the yellow and the magenta circles in Figures 1e) can also be trapped in the well and follow closed trajectories.

In other words, the trapping widths in θ and in energy depend on wave amplitude, which can be quantified by analyzing the separatrix (the black dashed lines in Figures 1a and 1e) between the trapped and untrapped trajectories. Since the separatrix must pass through the saddle point (the red dots in Figures 1a and 1e) at $\zeta = 180°$, $\theta = 0$, the C value in equation (12) for the separatrix must be ω_{tr}^2, and the separatrix is given by

$$\theta^2 = 2\omega_{tr}^2(1 + \cos\zeta). \tag{13}$$

Therefore, the minimum and maximum θ values for trapped electrons are $-2\omega_{tr}$ and $2\omega_{tr}$, respectively. The trapping width of $4\omega_{tr}$ in θ, according to (10), is proportional to the square root of the wave amplitude, which explains the difference between Figures 1a and 1e. Based on (5) and (4), the separatrices in the ζ-W and ζ-L spaces can be also obtained (see the black dashed lines in Figures 1b, 1c, 1f and 1g).

We next consider the manifestation of nonlinear wave-particle interactions and its difference from the conventional, linear picture. The effects of wave-particle interactions can be manifested by showing the particle energy gain δW from the waves as the function of W when the particle reaches a virtual spacecraft at a fixed location. To do so, we establish an ULF wave model, with the wave electric field (at the virtual spacecraft location) given in Figure 2a. Here we adopt essentially the same parameters as in Figure 1: the wave number $m = 75$, the wave period $T = 110$ s, the L-shell parameter of the virtual spacecraft is 6; the corresponding resonant energy is 54 keV at the spacecraft location. The only difference is that in this case, the wave amplitude grows exponentially from 0.2 mV/m at 0 s to 6 mV/m at 2000 s. This assumption is made to resemble the finite wave-particle interaction time (otherwise δW would depend on the initial ζ at $t = -\infty$, see discussions in *Southwood and Kivelson* [1981]). To compare the linear and nonlinear pictures, we next apply a linear approximation to determine δW by integrating (2) along the particle's unperturbed orbit backward in time to $t = -\infty$. The integration results, shown in Figure 2b in the format of δW energy spectrum, show characteristic signatures expected in *Southwood and Kivelson* [1981]: the δW oscillations are strongest at the resonant energy of 54 keV, and there appears a sharp, 180° phase shift across the resonant energy. The

nonlinear responses, shown in Figure 2d, suggest that very similar signatures (180°-phase shift) are still present when the wave electric field is relatively weak ($t < 700s$). As the wave amplitude continues to grow, however, rolled-up structures (unexpected from the linear theory) gradually appear around the resonant energy.

The formation of rolled-up structures, which have also been presented in the ϕ-L space [see *Degeling et al.*, 2007, Figure 3], can be better understood in Figure 3 showing the ζ-W phase space locations of a series of sample electrons (indicated by colored circles) as functions of time. All these electrons are launched at $t = 0$ with the initial energy of 54 keV (the resonant energy, indicated by the dashed lines), although their initial phases ζ are evenly distributed inside the potential well. The evolving shaded/non-shaded areas in Figure 3 correspond to the initial energies lower/higher than the resonant energy (and therefore having higher/lower PSDs if the PSD gradient over energy is negative at $t = 0$). The resonant electrons launched within the $-180° < \zeta < 0°$ and $0° < \zeta < -180°$ areas, as indicated in Figure 1, are immediately accelerated and decelerated, respectively. The accelerated/decelerated electrons, now above/below the dashed lines, would move to the right/left in addition to their vertical motions. The electron moving directions are also shown as arrows in Figure 3. It is the vortex-like motion of the electrons that generates rolled-up structures in the ζ-W phase space, which is centred near the bottom of the potential well at $\zeta \sim 0°$. One may also find that all these electrons gradually converge toward 0°; this is because of the increasing wave amplitude that enhances the trapping potential.

It is also of interest to examine the time it takes for the rolled-up structures to form. According to Figure 3, rolled-up structures become significant at $\sim$ 1000 s when most electrons (except for those launched near the edges of the potential well where small-angle approximation is invalid) have undergone half of their trapped motion (with their energies returning to the initial energy). In other words, the formation time of rolled-up structures should be about half of the particle trapping period $T_{tr} = 2\pi/\omega_{tr}$, although direct usage of (10) should be taken with caution in the formation time estimation since the wave amplitude E_ϕ is not constant. In fact, as E_ϕ grows, the decreasing T_{tr} suggests an increasing roll-up speed. For example, if we examine the followup behavior of the electrons that have just experienced half of the trapped motion at $\sim$ 1000 s, they will all finish one cycle of the trapped motion within the next 600 s (see Figure 3, bottom panel).

One may also analyze the electron responses to ULF waves with a finite lifespan. The wave electric field is given in Figure 2i, which differs from Figure 2a in that the wave growth rate is time-dependent (the wave growth and damping time scales are 90 s and 400 s, respectively). The resultant electron energy spectrum in Figure 2j, calculated based on a linear approximation, shows the presence of increasingly tilted stripes similar to the signatures described in *Zhou et al.* [2016]. If the nonlinear effects are considered (see Figure 2l), the tilted stripes gradually evolve into rolled-up structures soon after the wave amplitude peaks at t=400 s (about 200 s after the wave excitation).

We next convert the predicted δW spectrum into signatures observable from a realistic particle detector. The conversion from δW into variations of particle PSD, δf, can be

given by

$$\delta f = \delta W[\frac{L}{3W}\frac{\partial f(W,L)}{\partial L} - \frac{\partial f(W,L)}{\partial W}], \quad (14)$$

which is obtained based on the conservation of μ. According to (14), the PSD variation can be either in phase or in antiphase with δW depending on the signs of the PSD gradients in energy and in space. Here we follow *Zhou et al.* [2016] to utilize equation (14) with an assumed PSD profile in energy, and then consider a virtual detector with energy channels identical to those in the MagEIS (Magnetic Electron Ion Spectrometer) instrument [*Blake et al.*, 2013] on board Van Allen Probes [*Mauk et al.*, 2013]. This procedure converts Figures 2b and 2j into Figures 2c and 2k, which show the predicted energy spectrum of electron residual PSDs (based on linear approximation) in agreement with expectations in the conventional theory [*Southwood and Kivelson*, 1981; *Zhou et al.*, 2016]. It also converts Figures 2d and 2l into Figures 2e and 2m, which are the residual PSD spectra predicted from the nonlinear scenario.

One may find that Figures 2e and 2m are quite similar to those predicted in the linear approximation (Figures 2c and 2k). This is because of the limited energy resolution of the particle detector; the very fine, rolled-up structures in the nonlinear regime can hardly be recognized since electrons with different energies within a single energy channel have very different responses that cancel out in general (the phase mixing effect, see *Schulz and Lanzerotti* [1974]). The only discernible difference between the linear and nonlinear predictions appears in the channel near the resonant energy (54 keV); although both results show periodic oscillations at the wave frequency, only in the nonlinear results are there finer structures manifested as higher-frequency perturbations on top of the major,

periodic oscillations. These high-frequency perturbations can be better visualized after we apply a wavelet analysis on each energy channel (see Figures 2f-2h and 2n-2p for the wavelet power spectrum). All these wavelet spectra show a major peak at the period of 110 s (the ULF wave period), and there gradually appears a secondary peak at the period of $\sim$ 55 s (half of the wave period) especially in the near-resonant, 53.8-keV channel. The appearance of such high-frequency harmonics can be understood from the PSD structure in the bottom panel of Figure 3; the rolled-up structures (with PSD peaks represented by shaded areas) intersect the resonant energy (the horizontal dashed line) at two or three different locations within one wave cycle. In fact, the wavelet spectrum of the electron PSD oscillations may exhibit even higher harmonics as nonlinear wave-particle interactions continue (with greater wave amplitude or longer wave lifespan). These secondary peaks at the channel near the resonant energy may serve as diagnostic signatures (in the absence of particle data with higher energy resolution) indicating the presence of nonlinear drift resonance. These predicted signatures are to be compared in the next section with MagEIS data from Van Allen Probes observations.

3. Observations

In this section, the ULF wave event on 7 June 2014 is investigated based on Van Allen Probes observations. The electric field, magnetic field, and electron data are provided by the Electric Fields and Waves (EFW) [*Wygant et al.*, 2013], the Electric and Magnetic Field Instrument Suite and Integrated Science (EMFISIS) [*Kletzing et al.*, 2013], and the MagEIS [*Blake et al.*, 2013] instruments on Van Allen Probe A [*Mauk et al.*, 2013]. Figure 4a shows the electric field E_y and E_z components for this event. We make no attempt

to show the electric field E_x, since in this event the large $\left|\frac{B_y}{B_x}\right|$ and $\left|\frac{B_z}{B_x}\right|$ values result in a large uncertainty in the E_x determination via the $E \cdot B = 0$ approximation. Despite the lack of E_x data, the electric field measurements in Figure 4a clearly indicate excitation of ULF waves (with the period of $\sim$ 110 s) at approximately 1651:50 UT (the vertical dashed line). The dominant wave period of $\sim$ 110 s can be also seen in the wavelet power spectrum of E_y (Figure 4b).

Figure 4c shows the 90° pitch angle electron fluxes in each energy channel from 31.5 to 143.5 keV, which start to oscillate at about the same frequency as the ULF waves once the waves are excited. Figure 4d shows the energy spectrum of residual electron fluxes ($\frac{J-J_0}{J_0}$) during this time interval, where J are the original fluxes in each energy channel and J_0 are their sliding averages computed through an iterating scaled average algorithm [*Chen et al.*, 2016] (with the iteration number of 6 and a window width of 300 s). We then carry out a wavelet analysis on residual electron flux oscillations at the 31.5 keV, 53.8 keV, and 79.8 keV channels. The resultant wavelet power spectra, presented in Figures 4e-4g, all show a dominant period at 110 s (the same as the ULF wave period). At the 53.8-keV channel (Figure 4f), there is clearly a secondary peak at the period of $\sim$ 50 s (about half the period of the major peak), which starts to appear at $\sim$ 1653:30 UT (over 2 minutes after the ULF wave excitation). At other energy channels, the secondary peak hardly appears. These signatures are very similar to the predictions in Figures 2n-2p, which indicates the occurrence of nonlinear drift resonant process in this event. We also note that the secondary peak may alternatively be explained by particle interactions with higher-harmonic ULF waves. Although weak second-harmonic waves are indeed observed

at 1656:30 UT (see Figure 4b), this explanation is still quite unlikely since the secondary peak at the 53.8-keV channel appears 3 minutes earlier at 1653:30 UT. Also, if it is indeed the second-harmonic waves modulating the electrons, the secondary peak would have appeared in many different energy channels.

4. Summary and Discussions

Many recent studies on the ULF wave-particle interactions in the inner magnetosphere are largely based on the conventional drift resonance theory [*Southwood and Kivelson*, 1981, 1982; *Zhou et al.*, 2016], in which the wave-particle energy exchange is assumed small so the particle trajectories can be considered unperturbed. This linearization approach is not always accurate, however, especially when the energy changes of the resonant particles are comparable to their initial energies due to the large amplitude and/or lifespan of ULF waves [*Wang et al.*, 2018].

In this paper, we extend the conventional drift resonance theory into the nonlinear regime. We formulate the nonlinear trapping of charged particles with a pendulum equation, and accordingly determine the period and width of the trapping motion. Besides describing the particle behavior during this process, we also predict the characteristic signatures of the nonlinear drift resonance, which are different from those in the linear approximation. We expect to see rolled-up structures in the particle energy spectrum (given sufficiently high energy resolution of the particle data), which result from the trapping of resonant particles in the wave-carried potential well. The time it takes for the rolled-up structures to form is closely related to the trapping period T_{tr} of the resonant particles within the potential well. According to (10), this formation time is inversely

proportional to the square root of the amplitude of the wave electric field. In other words, the structures will roll up faster given a larger wave amplitude. We also examine the manifestations of nonlinear drift resonance observable from a MagEIS-type particle detector with a limited energy resolution. In this case, the rolled-up structures may be masked by the phase mixing effect. In the absence of high resolution data, the most characteristic signatures of nonlinear drift resonance are the multi-period oscillations in the energy channel near the resonant energy. These predicted signatures are indeed observed by Van Allen Probes, which provides a first observational evidence over the occurrence of nonlinear drift resonance and highlights the importance of nonlinear effects in the understanding of ULF wave-particle interactions in the inner magnetosphere.

Finally, we note that there remains a few assumptions that may require further development of the theory. In this study, we only deal with nonrelativistic particles, and it would be natural to extend the theory into relativistic particles in a followup study. Also, the conversion from δW to δf is still based on the linear assumption (14) that the PSD gradients in energy and space are constant even if the particle experiences significant variations in W and L. This assumption can be easily relaxed by adopting a more realistic, equilibrium model of particle PSD profiles as the initial condition. For any given particle that reaches the virtual spacecraft, the corresponding PSD at any time can be obtained via Liouville's theorem once we compute its W and L variations. Therefore, these minor adjustments would not significantly change our prediction on the characteristic signatures of nonlinear drift resonance. One may also notice from (1) that the modeled wave amplitude is independent on L or ϕ, which is not real in Earth's magnetosphere. Given a

finite radial scale of ULF waves, our scenario may require adjustments if particle's radial displacement is large compared to half width of the wave excitation [*Wang et al.*, 2018]. The azimuthal scale of ULF waves, as discussed in *Degeling et al.* [2007], could provide an inhomogeneity factor for the pendulum equation to enable significant particle scattering [*Tobita and Omura*, 2018]. Similar effects may also appear if a convective electric field is introduced to the model. These further developments will be addressed in a future study.

Acknowledgments. This study was supported by NSFC grants 41774168, 414221003 and 41474140. Y. O. acknowledges support from JSPS KAKENHI grant 17H06140, and R. R. acknowledges support from Canadian Space Agency and NSERC. The Van Allen Probes data used in this study can be accessed from NASA′s Space Physics Data Facility at http://spdf.gsfc.nasa.gov/.

References

Anderson, B. J., M. J. Engebretson, S. P. Rounds, L. J. Zanetti, and T. A. Potemra (1990), A statistical study of Pc 3-5 pulsations observed by the AMPTE/CCE Magnetic Fields Experiment, 1. Occurrence distributions, *J. Geophys. Res.*, *95*, 10,495–10,523, doi:10.1029/JA095iA07p10495.

Blake, J. B., et al. (2013), The Magnetic Electron Ion Spectrometer (MagEIS) Instruments Aboard the Radiation Belt Storm Probes (RBSP) Spacecraft, *Space Sci. Rev.*, *179*, 383–421, doi:10.1007/s11214-013-9991-8.

Chen, L., and A. Hasegawa (1974), A theory of long-period magnetic pulsations: 1. Steady state excitation of field line resonance, *J. Geophys. Res.*, *79*, 1024–1032, doi:

10.1029/JA079i007p01024.

Chen, X.-R., Q.-G. Zong, X.-Z. Zhou, J. B. Blake, J. R. Wygant, and C. A. Kletzing (2016), Van allen probes observation of a 360° phase shift in the flux modulation of injected electrons by ulf waves, *Geophysical Research Letters*, doi:10.1002/2016GL071252.

Chen, Y., G. D. Reeves, and R. H. W. Friedel (2007), The energization of relativistic electrons in the outer Van Allen radiation belt, *Nature Phys.*, *3*, 614–617, doi:10.1038/nphys655.

Claudepierre, S. G., et al. (2013), Van Allen Probes observation of localized drift resonance between poloidal mode ultra-low frequency waves and 60 keV electrons, *Geophys. Res. Lett.*, *40*, 4491–4497, doi:10.1002/grl.50901.

Cummings, W. D., R. J. O'Sullivan, and P. J. Coleman Jr. (1969), Standing alfven waves in the magnetosphere, *J. Geophys. Res.*, *74*, 778–793.

Dai, L., et al. (2013), Excitation of poloidal standing Alfven waves through drift resonance wave-particle interaction, *Geophys. Res. Lett.*, *40*, 4127–4132, doi:10.1002/grl.50800.

Degeling, A. W., R. Rankin, K. Kabin, R. Marchand, and I. R. Mann (2007), The effect of ULF compressional modes and field line resonances on relativistic electron dynamics, *Planet. Space Sci.*, *55*, 731–742, doi:10.1016/j.pss.2006.04.039.

Degeling, A. W., L. G. Ozeke, R. Rankin, I. R. Mann, and K. Kabin (2008), Drift resonant generation of peaked relativistic electron distributions by Pc 5 ULF waves, *J. Geophys. Res.*, *113*, A02208, doi:10.1029/2007JA012411.

Elkington, S. R., M. K. Hudson, and A. A. Chan (2003), Resonant acceleration and diffusion of outer zone electrons in an asymmetric geomagnetic field, *J. Geophys. Res.*,

108, 1116, doi:10.1029/2001JA009202.

Foster, J. C., J. R. Wygant, M. K. Hudson, A. J. Boyd, D. N. Baker, P. J. Erickson, and H. E. Spence (2015), Shock-induced prompt relativistic electron acceleration in the inner magnetosphere, *J. Geophys. Res.*, *120*, 1661–1674, doi:10.1002/2014JA020642.

Gurnett, D. A., and A. Bhattacharjee (2005), *Introduction to Plasma Physics*, Cambridge University Press, Cambridge, UK.

Hao, Y. X., et al. (2017), Relativistic electron dynamics produced by azimuthally localized poloidal mode ULF waves: Boomerang-shaped pitch angle evolutions, *Geophys. Res. Lett.*, *44*, 7618–7627, doi:10.1002/2017GL074006.

Horne, R. B., et al. (2005), Wave acceleration of electrons in the Van Allen radiation belts, *Nature*, *437*, 227–230, doi:10.1038/nature03939.

Kivelson, M. G., and D. J. Southwood (1985), Resonant ULF waves - A new interpretation, *Geophys. Res. Lett.*, *12*, 49–52, doi:10.1029/GL012i001p00049.

Kletzing, C. A., et al. (2013), The Electric and Magnetic Field Instrument Suite and Integrated Science (EMFISIS) on RBSP, *Space Sci. Rev.*, *179*, 127–181, doi:10.1007/s11214-013-9993-6.

Li, L., X. Z. Zhou, Q. G. Zong, X. R. Chen, H. Zou, J. Ren, Y. X. Hao, and X. G. Zhang (2017), Ultralow frequency wave characteristics extracted from particle data: Application of IGSO observations, *Sci. China Tech. Sci.*, *30*, 1–6, doi:10.1007/s11431-016-0702-4.

Li, L., X.-Z. Zhou, Q.-G. Zong, R. Rankin, H. Zou, Y. Liu, X.-R. Chen, and Y.-X. Hao (2017), Charged particle behavior in localized ultralow frequency waves: Theory and

observations, *Geophys. Res. Lett.*, *44*, 5900–5908, doi:10.1002/2017GL073392.

Li, W., et al. (2014), Radiation belt electron acceleration by chorus waves during the 17 March 2013 storm, *J. Geophys. Res.*, *119*, 4681–4693, doi:10.1002/2014JA019945.

Liu, W., W. Tu, X. Li, T. Sarris, Y. Khotyaintsev, H. Fu, H. Zhang, and Q. Shi (2016), On the calculation of electric diffusion coefficient of radiation belt electrons with in situ electric field measurements by THEMIS, *Geophys. Res. Lett.*, *42*, doi: 10.1029/2015GL067398.

Mann, I. R., et al. (2013), Discovery of the action of a geophysical synchrotron in the Earth's Van Allen radiation belts, *Nature Comm.*, *4*, 2795, doi:10.1038/ncomms3795.

Mauk, B. H., N. J. Fox, S. G. Kanekal, R. L. Kessel, D. G. Sibeck, and A. Ukhorskiy (2013), Science objectives and rationale for the radiation belt storm probes mission, *Space Sci. Rev.*, *179*, 3–27, doi:10.1007/s11214-012-9908-y.

Northrop, T. G. (1963), Adiabatic Charged-Particle Motion, *Rev. Geophys.*, *1*, 283–304, doi:10.1029/RG001i003p00283.

Sarris, T. E., X. Li, M. Temerin, H. Zhao, S. Califf, W. Liu, and R. Ergun (2017), On the relationship between electron flux oscillations and ULF wave-driven radial transport, *Journal of Geophysical Research (Space Physics)*, *122*, 9306–9319, doi: 10.1002/2016JA023741.

Schulz, M., and L. J. Lanzerotti (1974), Particle Diffusion in the Radiation Belts, in *Physics and Chemistry in Space*, vol. 7, p. 215, Springer-Verlag, New York.

Southwood, D. J. (1974), Some features of field line resonances in the magnetosphere, *Planet. Space Sci.*, *22*, 483–491, doi:10.1016/0032-0633(74)90078-6.

Southwood, D. J., and M. G. Kivelson (1981), Charged particle behavior in low-frequency geomagnetic pulsations: I. Transverse waves, *J. Geophys. Res.*, *86*, 5643–5655.

Southwood, D. J., and M. G. Kivelson (1982), Charged particle behavior in low-frequency geomagnetic pulsations. II - Graphical approach, *J. Geophys. Res.*, *87*, 1707–1710.

Summers, D., R. M. Thorne, and F. Xiao (1998), Relativistic theory of wave-particle resonant diffusion with application to electron acceleration in the magnetosphere, *J. Geophys. Res.*, *103*, 20,487–20,500, doi:10.1029/98JA01740.

Takahashi, K., and R. L. McPherron (1984), Standing hydromagnetic oscillations in the magnetosphere, *Planet. Space Sci.*, *32*, 1343–1359.

Tobita, M., and Y. Omura (2018), Nonlinear dynamics of resonant electrons interacting with coherent Langmuir waves, *Phys. Plasmas*, *25*(3), 032105, doi:10.1063/1.5018084.

Wang, C., R. Rankin, Y. Wang, Q.-G. Zong, X.-Z. Zhou, K. Takahashi, R. Marchand, and A. W. Degeling (2018), Poloidal Mode Wave-Particle Interactions Inferred From Van Allen Probes and CARISMA Ground-Based Observations, *J. Geophys. Res. Space Physics*, *123*, doi:10.1002/2017JA025123.

Wygant, J. R., et al. (2013), The Electric Field and Waves Instruments on the Radiation Belt Storm Probes Mission, *Space Sci. Rev.*, *179*, 183–220, doi:10.1007/s11214-013-0013-7.

Zhou, X.-Z., Z.-H. Wang, Q.-G. Zong, R. Rankin, M. G. Kivelson, X.-R. Chen, J. B. Blake, J. R. Wygant, and C. A. Kletzing (2016), Charged particle behavior in the growth and damping stages of ultralow frequency waves: Theory and Van Allen Probes observations, *J. Geophys. Res.*, *121*, 3254–3263, doi:10.1002/2016JA022447.

Zhou, X.-Z., et al. (2015), Imprints of impulse-excited hydromagnetic waves on electrons in the Van Allen radiation belts, *Geophys. Res. Lett.*, *42*, 6199–6204, doi: 10.1002/2015GL064988.

Zong, Q., R. Rankin, and X. Zhou (2017), The interaction of ultra-low-frequency pc3-5 waves with charged particles in Earth's magnetosphere, *Reviews of Modern Plasma Physics*, *1*, 10, doi:10.1007/s41614-017-0011-4.

Zong, Q.-G., et al. (2007), Ultralow frequency modulation of energetic particles in the dayside magnetosphere, *Geophys. Res. Lett.*, *34*, 12,105, doi:10.1029/2007GL029915.

Zong, Q.-G., et al. (2009), Energetic electron response to ULF waves induced by interplanetary shocks in the outer radiation belt, *J. Geophys. Res.*, *114* (A13), A10204, doi:10.1029/2009JA014393.

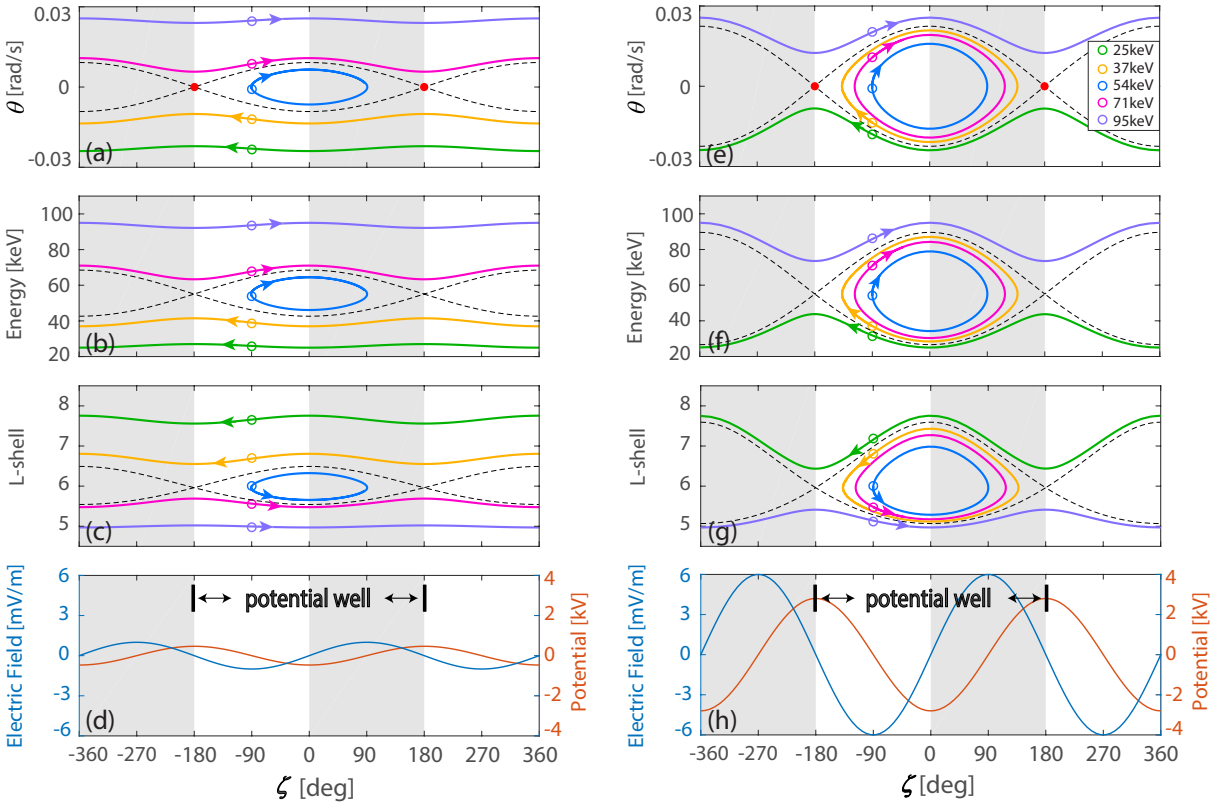

Figure 1. Phase portrait of sample electron trajectories in the ULF wave field. The left and the right columns correspond to the cases with different wave amplitudes. The horizontal axis represents ζ, the phase of electron location in the rest frame of the waves. The vertical axes (from top to the third panels) represents θ, electron energy, and L location, respectively. The bottom panels show the profiles of the wave electric field and the corresponding electrostatic potential.

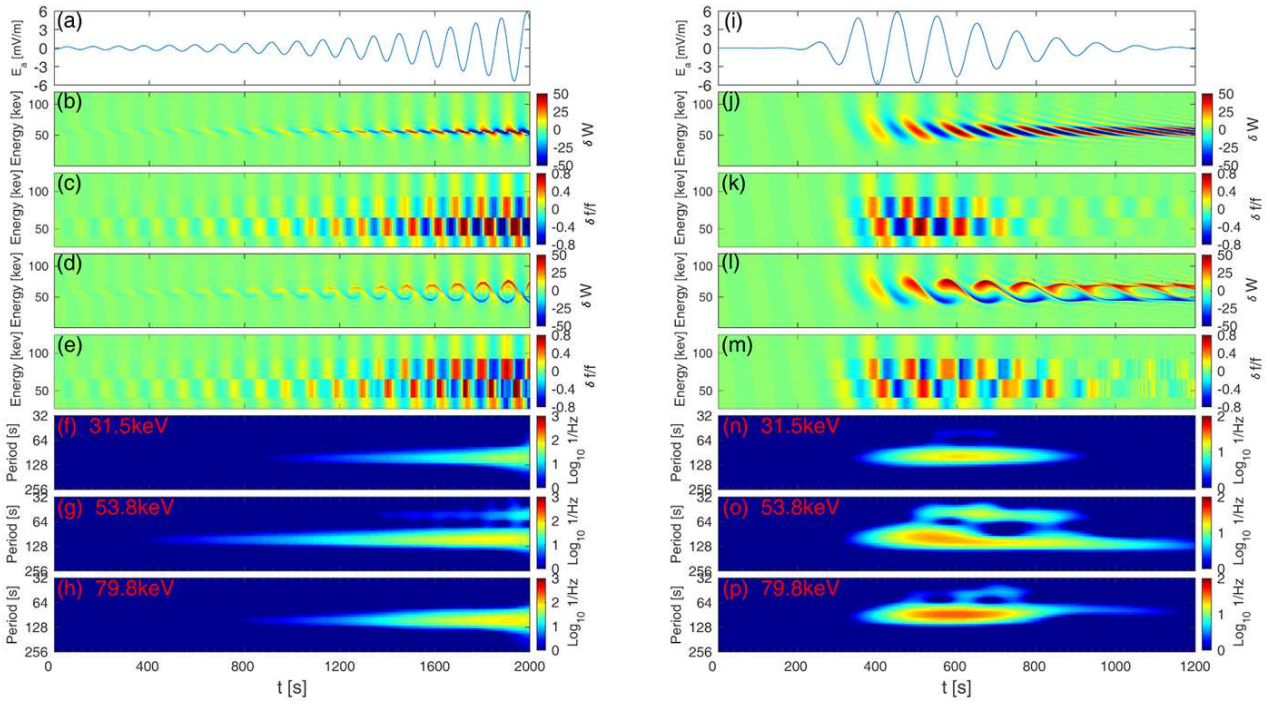

Figure 2. Predicted electron signatures at a fixed, virtual spacecraft location. The left and right columns correspond to ULF waves with increasing amplitudes and with a finite lifespan, respectively. (a,i) The wave electric field; energy spectrum of the electron energy gain/loss from ULF waves, obtained from (b,j) the linear and (d,l) the nonlinear theories; energy spectrum of the electron residual PSD at each energy channel, obtained from (c,k) the linear and (e,m) the nonlinear theories; (f-h,o-p) wavelet power spectrum of the electron residual PSD obtained from the nonlinear theory, in the 31.5 keV, 53.8 keV, and 79.8 keV energy channels.

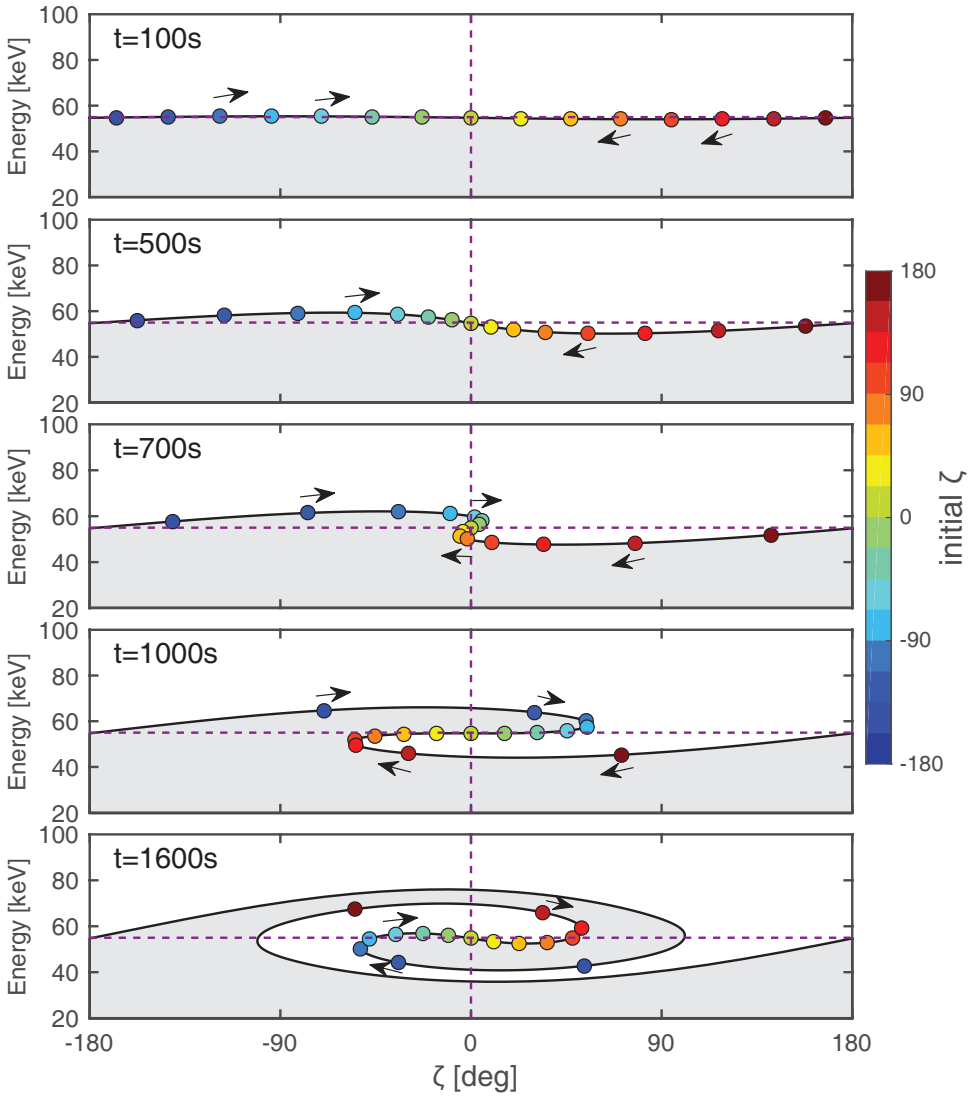

Figure 3. Evolution of the electron phase-space locations after the sample electrons are launched in the ULF wave field at the resonant energy (54 keV). The corresponding ULF wave electric field is given in Figure 2a.

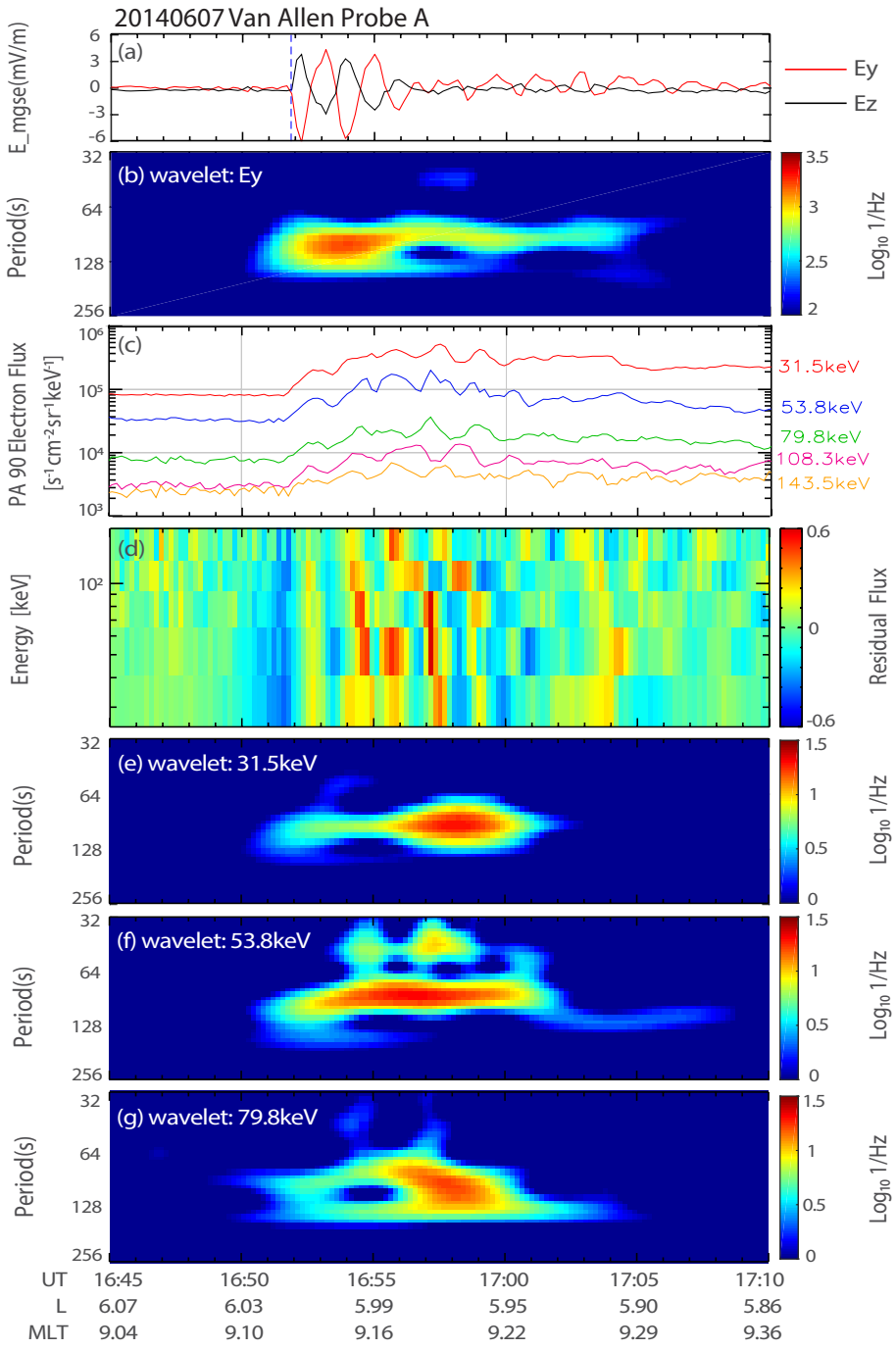

Figure 4. Van Allen Probe A observations of an ULF wave event on 7 June 2014. (a) The electric field E_y and E_z; (b) wavelet power spectrum of E_y; (c) 90°-pitch angle electron fluxes at multiple energy channels; (d) energy spectrum of the electron residual fluxes; (e-g) wavelet power spectrum of electron residual fluxes in the 31.5 keV, 53.8 keV, and 79.8 keV energy channels.

Figure 1.

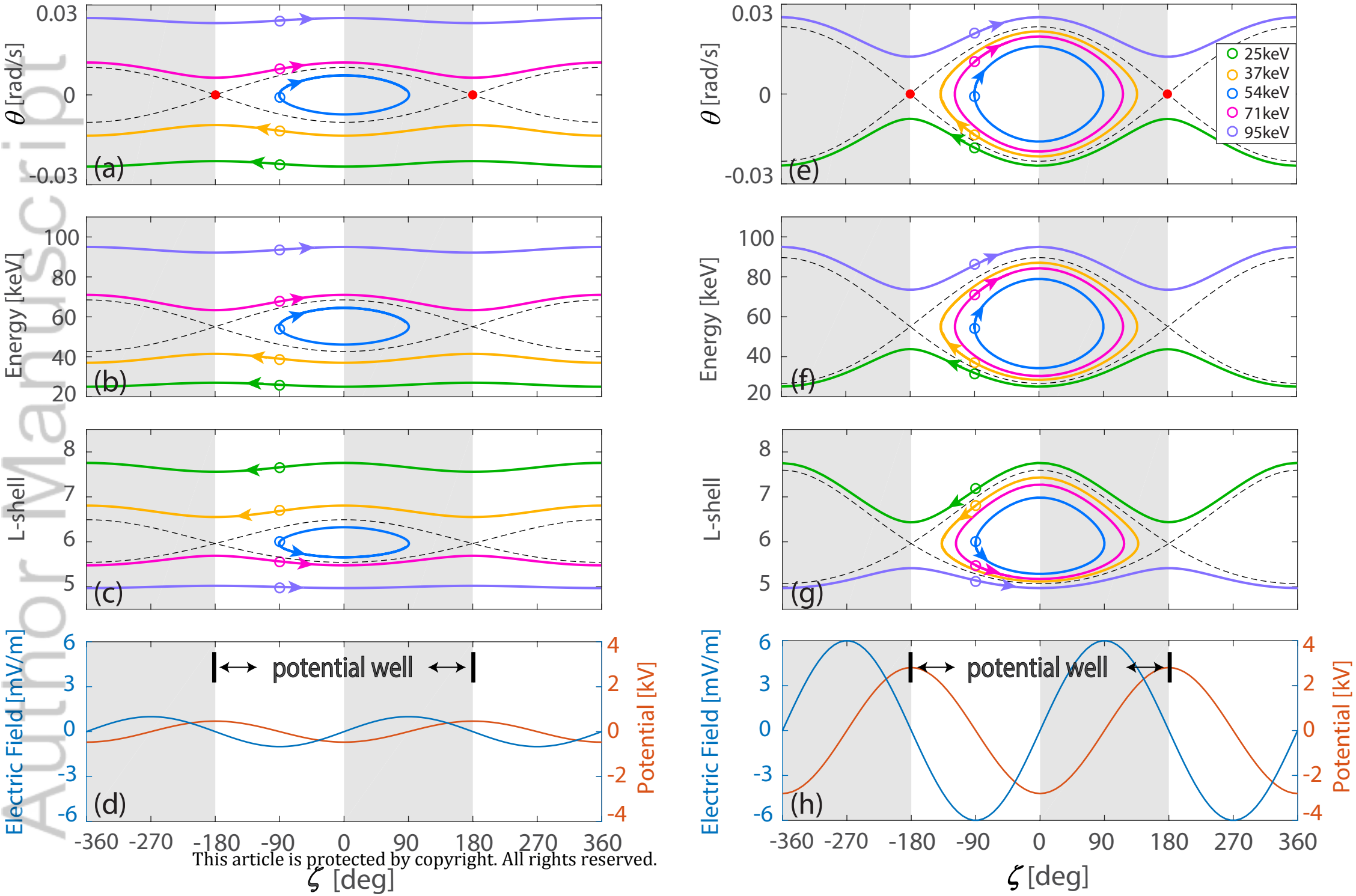

Figure 2.

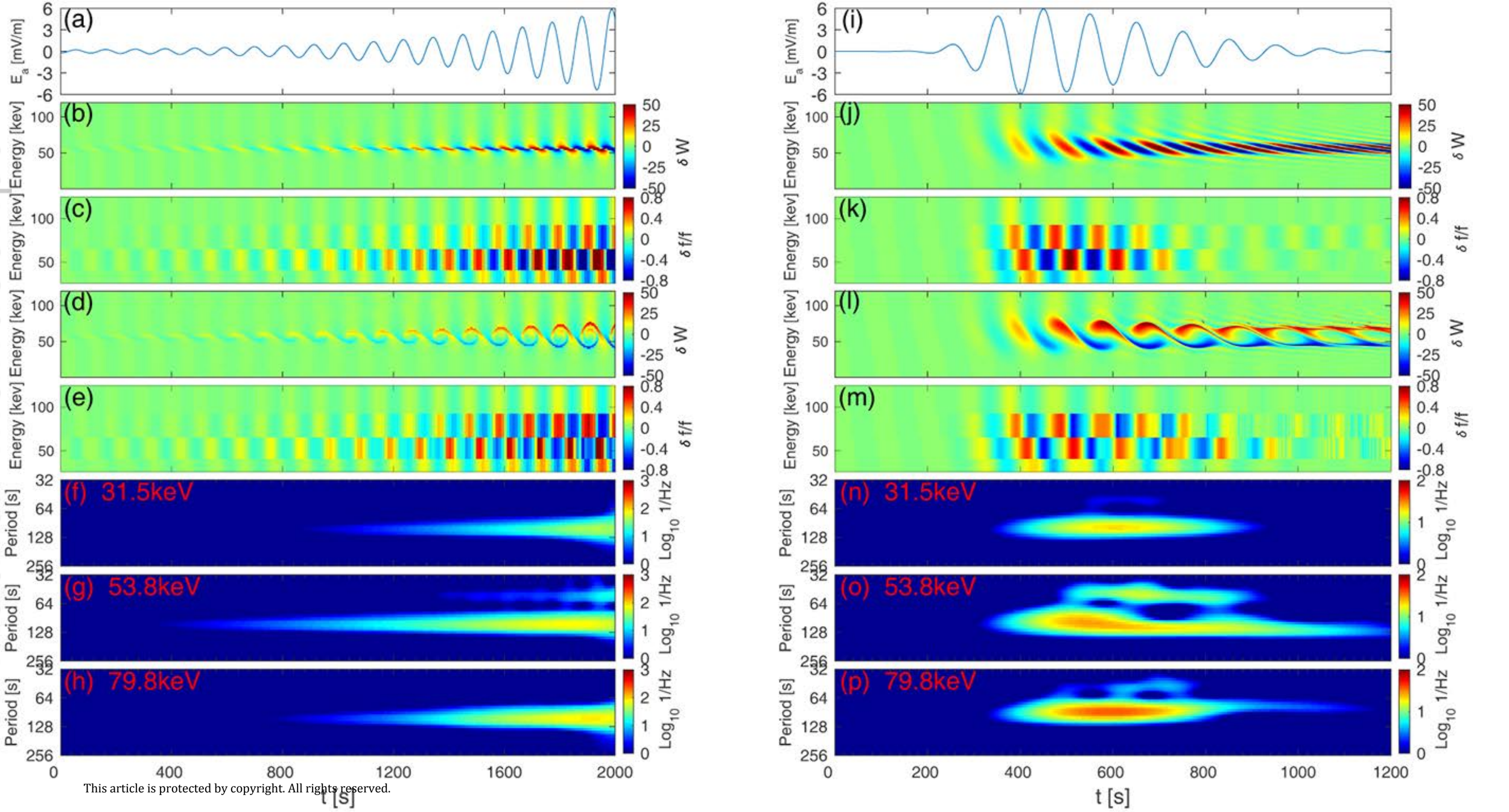

Figure 3.

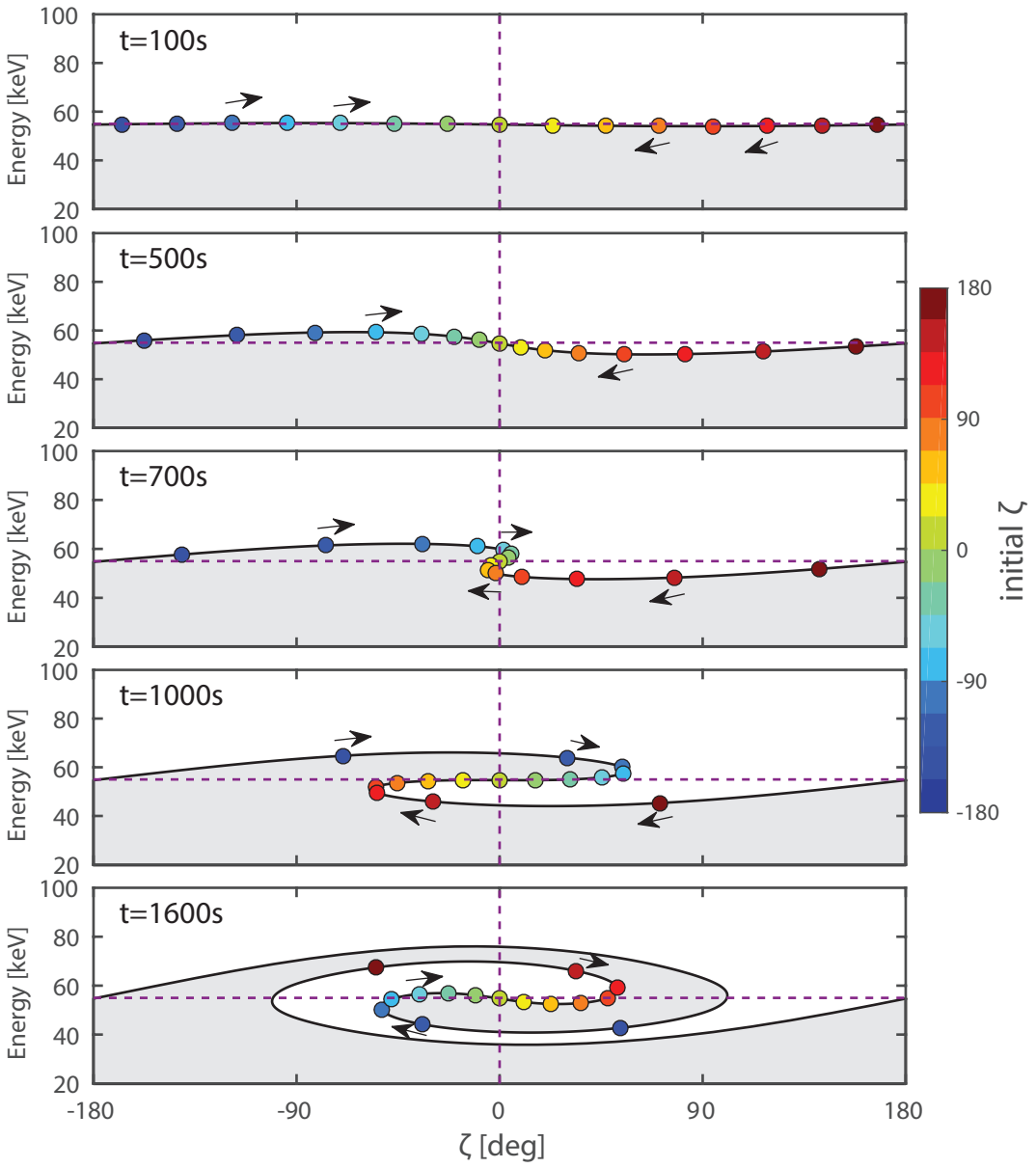

Figure 4.

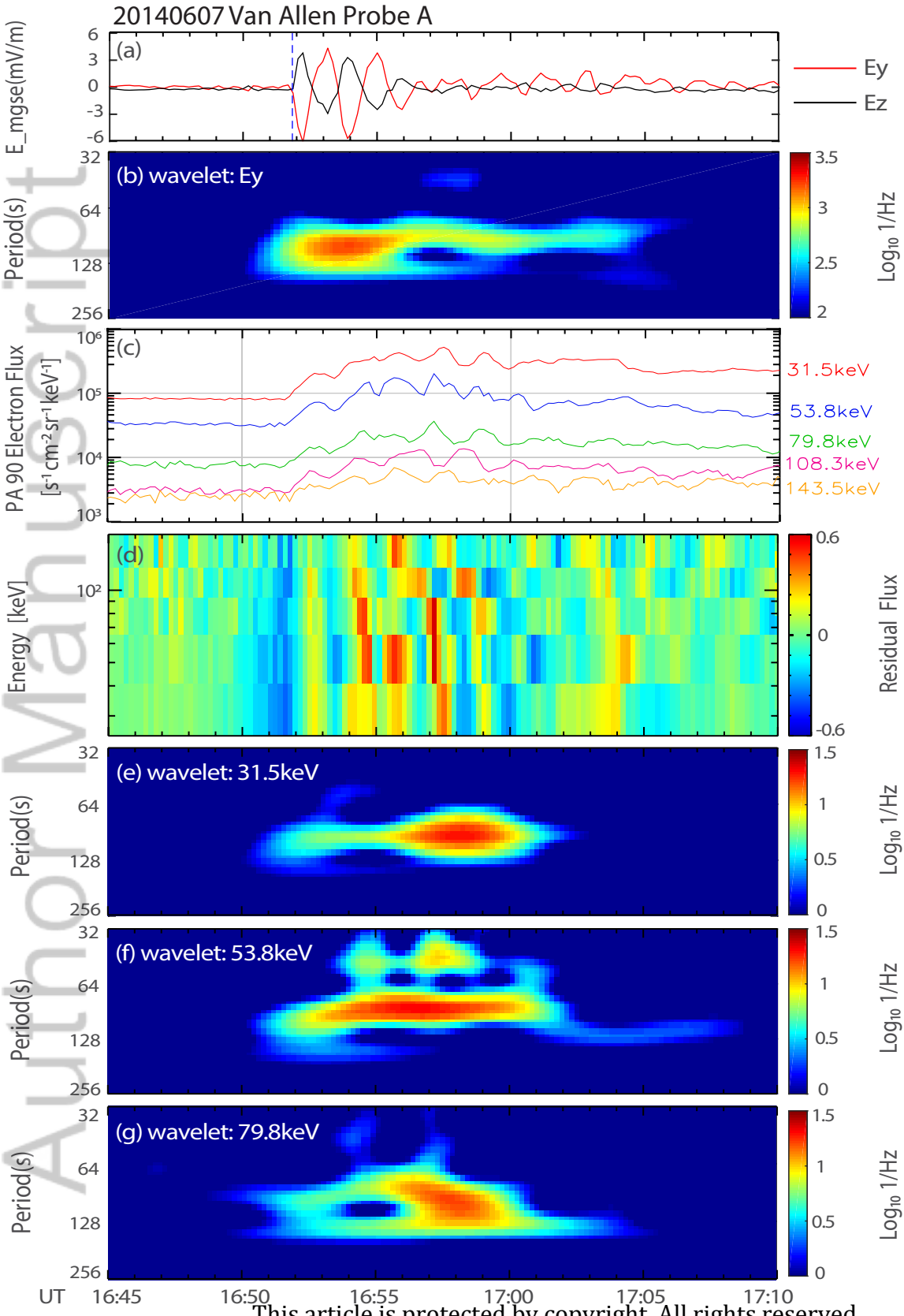

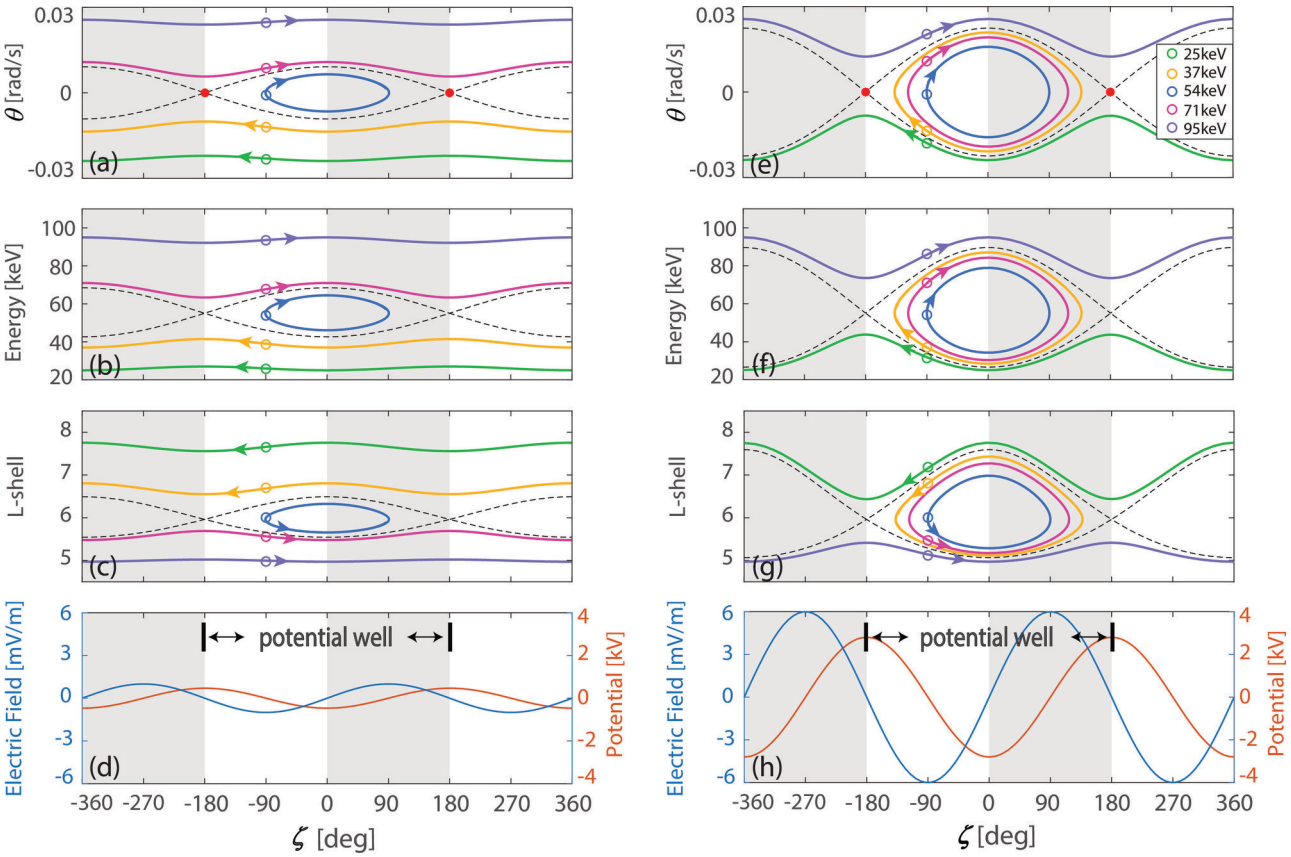

2018gl079038-f01-z-.eps

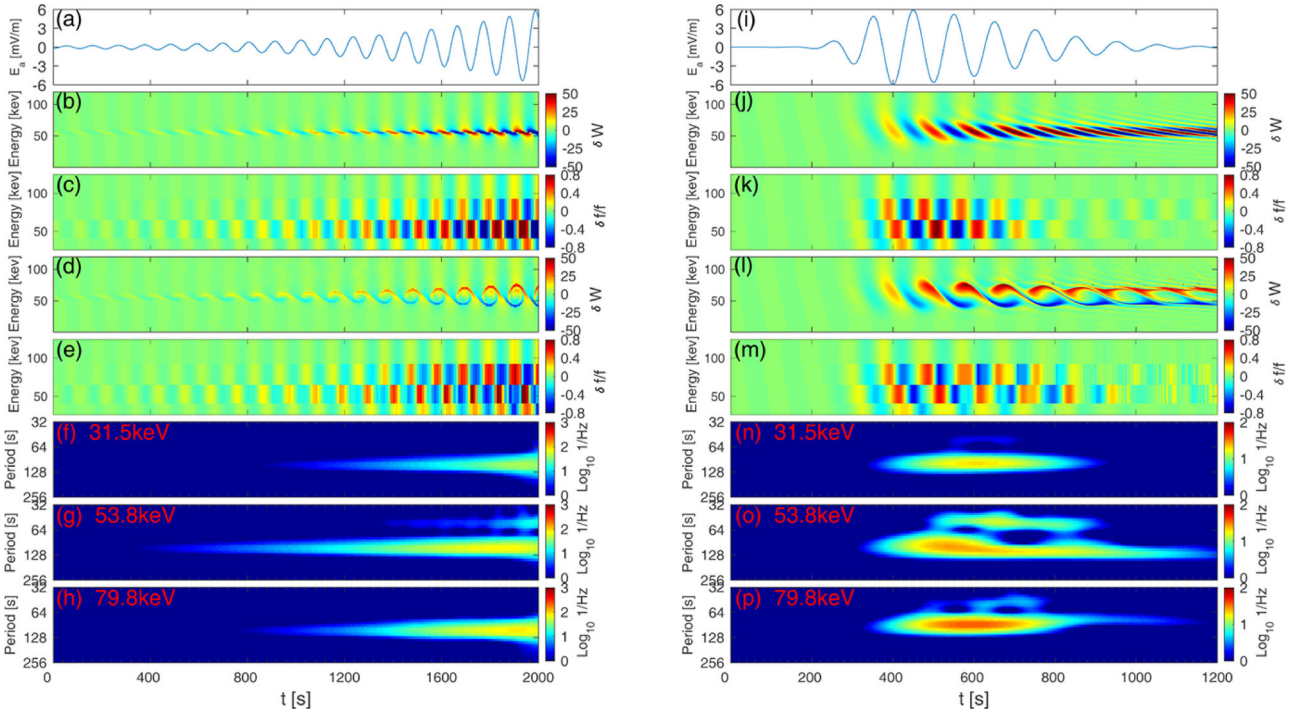

2018gl079038-f02-z-.eps

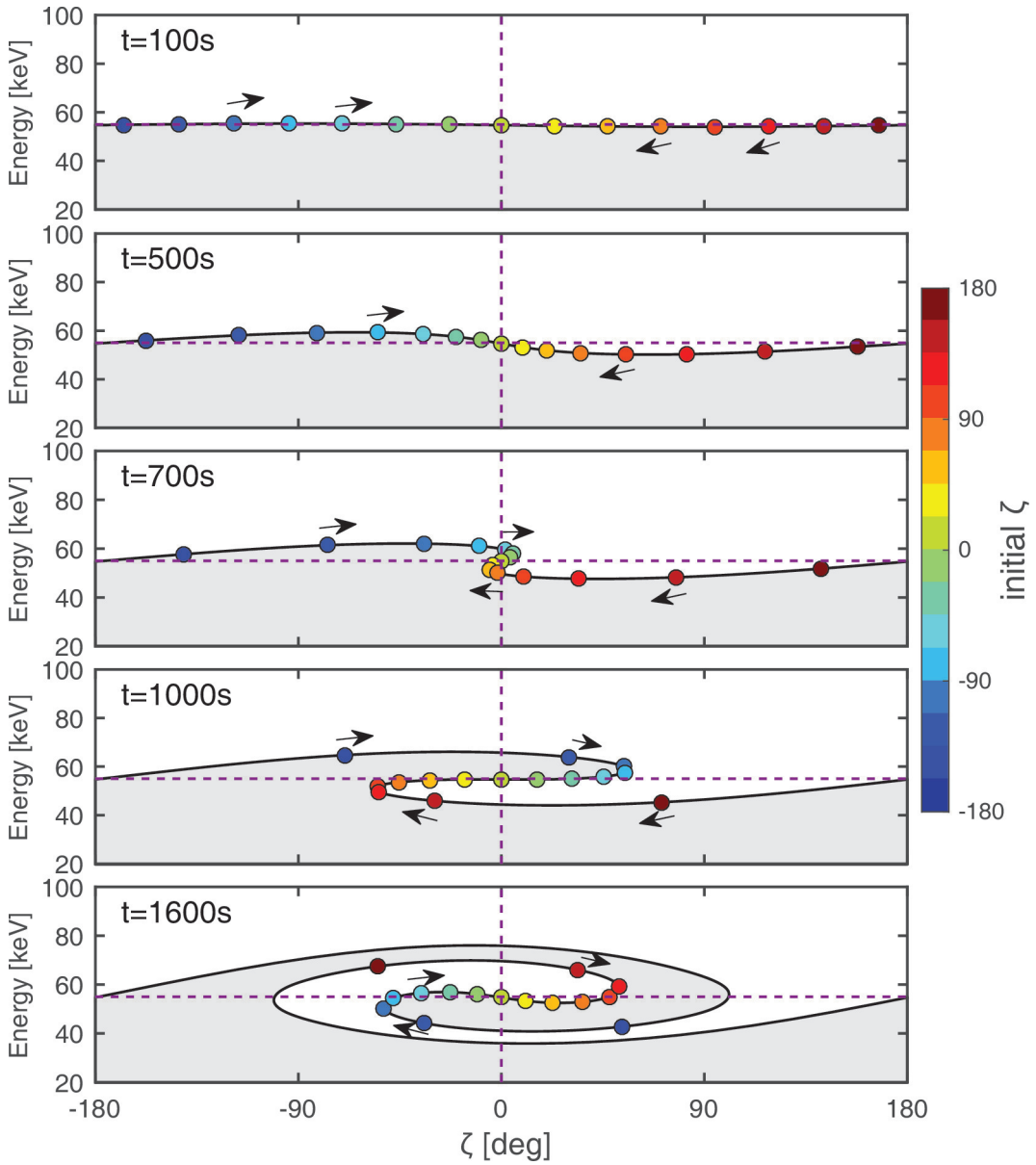

2018gl079038-f03-z-.eps

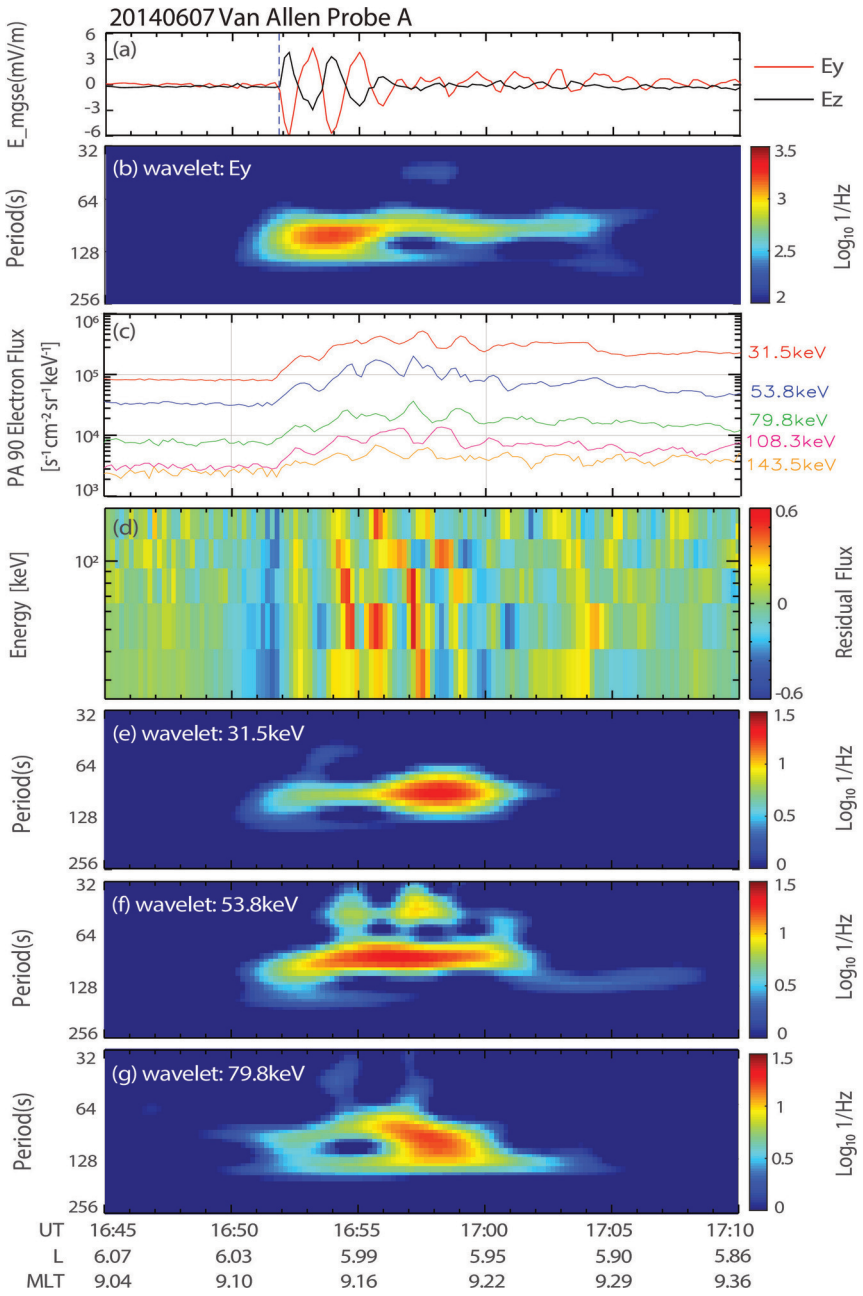

2018gl079038-f04-z-.eps